Vector vortex beams generation and classification via photonic quantum walks and deep-learning

Temporary author list

Taira Giordani, Alessia Suprano, Emanuele Polino, Francesca Acanfora, Nicoló Spagnolo, and Fabio Sciarrino
Dipartimento di Fisica, Sapienza Università di Roma, Piazzale Aldo Moro 5, I-00185 Roma, Italy

Belfast
Centre for Theoretical Atomic, Molecular, and Optical Physics,
School of Mathematics and Physics, Queen's University Belfast, BT7 1NN Belfast, United Kingdom

Lorenzo Marrucci
Università Federico II, Complesso Universitario di Monte Sant'Angelo, Via Cintia, 80126 Napoli, Italy

In recent years structured light has attracted notable attention for the several applications in classical and quantum optics fields. In particular, the so called vector vortex beams display peculiar properties in both regimes, due to the non-trivial correlations existing between polarization and orbital angular momentum. Here we reaffirm their pivotal role providing a new flexible technique for preparation and classification of different vector vortex beams. Firstly we propose a novel platform for generating arbitrary complex vector vortex beams inspired to photonic quantum walks. Secondly, we exploit recent deep-learning methods, namely convolutional neural networks, to recognize and classify specific polarization patterns.

Introduction—A vector vortex beam (VVB) is a particular mode of the electromagnetic field in which the polarization is not uniform in the transverse plane. Examples of VVBs are obtainable by coherent superposition of so called Laguerre-Gauss (LG) and Hermite-Gauss (HG) modes, namely orthonormal family of solution of the Helmholtz equation in the paraxial approximation, with orthogonal polarizations. In literature is usual to refer to such beams as *vortex* since the resulting wavefront has the characteristic elichoidal shape. The interest in such beams is motivated by the multiple applications in different field of optics, from the classical to the quantum regime. In the first context, VVBs display special behaviours under focusing [1–3], making them optimal to cut metals [4, 5], to beat the diffraction limits for purposes in microscopy, to trap particle, only to mention a few. For instance, at the focal point, a beam with radial polarization possess a strong longitudinal electric field and a small spot size, a beam with azimuthal polarization possess a smaller spot focal size but a strong azimuthal electric field. Furthermore VVBs are quite employed in quantum information protocols for the correlations between polarization and spatial modes of single photons. Different photonic platform based on the encoding of information in these degrees of freedom have been implemented in several experiments for quantum sensing and metrology [6, 7], quantum communication and cryptography [8–11], in phtonics quantum walks [12, 13] for quantum simulations [14, 15] and for quantum state engineering [16].

Motivated by the trasversal role of VVB in optics, is still crucial to provide a reliable technique to generate and classify different optical vector fields. Recently, machine learning techniques have became a common tool for many tasks in different areas, demonstrating to be an useful add-on to the experimental platforms, helping for characterizations and automation. Regarding structured light in optics, in previous works artificial neural network (ANN) and convolutional neural network (CNN) have been employed for demultiplexing orbital angular momentum (OAM) components, namely different LG modes, in protocols for communication in free space [10, 11, 17–22]. In this work we apply for the first time such approach to VVBs which have been generated in a novel platform inspired partially to photonics quantum walks (QWs) in the OAM degree of freedom. Indeed in recent years many techniques for generating VVBs have been developed. Previous methods manipulate properly a laser in a resonator to generate the desired vector pattern [4]. Others exploit interferometric schemes, diffraction from sub-wavelength gratings or holograms and through passes into inhomogeneous birefringent media such *q-plates* [23]. However the main drawback of these methods is that they could address the generation of just particular VVBs. Then, respect to previous techniques, our approach is flexible for generating several types of VVB, not only limited to radial and azhimutal polarized vector fields. The platform is a generalization of the scheme proposed in Ref. [23] in which it is possible to generate arbitrary vectorial fields with cascaded q-plates and waveplates set, exploiting the possibility to manipulate both polarization and LG modes. The resulting platform resembles photonics quantum walks in the OAM [13–16], offering a further application of the model not only in the quantum regime, but also for generating structured light as VVBs.

Our results confirm the feasibility of this novel approach for generating high-order Poincaré sphere usually associated to VVB, in which two LG mode carrying different OAM are superposed coherently with different polarizations. Furthermore a CNN, built specifically for the experiment, enables for classifying firstly the vortex associated to unitary OAM and spin angular momentum (SAM) in its Poincaré Sphere and then to retrieve the value of OAM in the more general case,

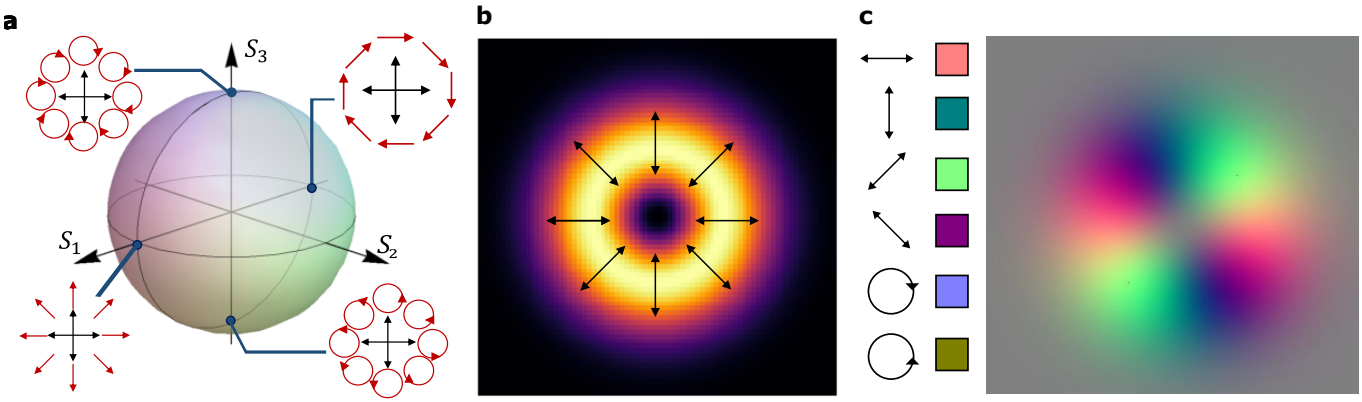

Figure 1. a) High-order Poincarré sphere representation for $|m_1| = |m_2| = 1$. At each point on the sphere surface corresponds a specific polarization patterns. The radial and azimutal VVBs, the most interesting for their properties under focusing, corresponds to the position $\theta = \frac{\pi}{2}$, $\phi = 0$ and $\frac{\pi}{2}$ respectively. b) Insight to a VVB radially polarized. At a given point in the trasversal plane the polarization vector has a different orientation. Then also the Stokes parameters vary properly in the plane. c) Encoding of the polarization pattern in different colors. Given the set of Stokes parameters $S = \{S_1, S_2, S_3\}$ it is possible to convert it in a RGB color. In the legend is reported the correspondence between colors and horizontal, vertical, diagonal, anti-diagonal, left and right circular polarization. On the right we have the resulting color pattern for VVB showed in b). Grey corresponds to unpolarized light.

with superposition of arbitrary LG modes. In this way we demonstrate a robust and reliable method for the generation and recognition of VVBs, that can be at the basis for different automatized quantum information and communication protocols.

Vector vortex beam generation— Let us define the formalism of VVB that we will use throughout this work. The electromagnetic field carries angular momentum in the form of SAM component, related to its vectorial nature, namely polarization, and OAM, that, instead is linked to the shape of wavefront. The LG modes carry a precise amount of orbital angular momentum, that in the single photon regime is equal to $m\hbar$ [24]. Indeed such solution of the Helmholtz equation are described by two integer numbers, $m \in \mathbb{Z}$ for the azimutal degree of freedom and the $p \in \mathbb{N}$ for the radial part. A VVB consists of a coherent superposition of two LG mode with different azimutal order, namely m_1 and m_2 with $m_1 > m_2$, and the same p, with orthogonal polarization:

$$\vec{E}_{m_1 m_2 p} = \vec{e}_L \cos\frac{\theta}{2}\,\mathrm{LG}_{m_1 p} + \vec{e}_R e^{i\phi} \sin\frac{\theta}{2}\,\mathrm{LG}_{m_2 p}, \quad (1)$$

where the versors $\{\vec{e}_L, \vec{e}_R\}$ correspond to left and right circular polarization. For the purpose of this work it is possible to ignore the radial number, fixing $p = 0$. According to equation (1), VVBs can be mapped, for fixed a set of (m_1, m_2) on a generalized Poincarré sphere, according to the parameters θ and ϕ [25]. As showed in Fig.1a for the case $|m_1| = |m_2| = 1$, each polarization pattern corresponds to a position on the sphere. Hence it can be reconstructed by means of measurement of the Stokes parameters which allows to determinate unambiguously the order of the Poincarré sphere, namely m_1 and m_2, and eventually the position, θ and ϕ. Stokes parameters are obtainable projecting the state to the three unbaised basis for the polarization degree of freedom, $b = \{(H, V), (D, A), (L, R)\}$. In such way Stokes parameters, which corresponds to the position into the Poincarré sphere, are defined as follows:

$$\begin{aligned} S_1 &= \frac{I_H - I_V}{I_H + I_V} \\ S_2 &= \frac{I_D - I_A}{I_D + I_A} \\ S_3 &= \frac{I_R - I_L}{I_R + I_L} \end{aligned} \quad (2)$$

where I_b stands for the intensity measured for the polarization specified in the subscripts. The polarization pattern results in different values of the set $S = \{S_1, S_2, S_3\}$ for each point (x, y) of the transverse plane (we have fixed implicitly the axis of propagation along z). In this work we propose an encoding of polarization patterns identifying a VVB based on a color map. The set S is converted in a particular color according to the RGB encoding. In Fig.1b and c is showed the resulting color map for a radially polarized optical vortex.

Experimental apparatus— A natural way for generating different VVBs is through *q-plates* [23, 26], inhomegenous birifringent plates able to generate LG_m modes according to the polarization state. In particular, named q the topological charge of the device, we have

$$\begin{aligned} \vec{e}_L\ \mathrm{LG}_m &\xrightarrow{\mathrm{QP}} \vec{e}_R\ \mathrm{LG}_{m+2q} \\ \vec{e}_R\ \mathrm{LG}_m &\xrightarrow{\mathrm{QP}} \vec{e}_L\ \mathrm{LG}_{m-2q} \end{aligned} \quad (3)$$

Our scheme for generating VVB states is based on concepts of discrete-time quantum walk in the OAM degree of freedom. In this paradigm the order of LG modes is increased or decreased according to the polarization state [12, 13, 27]. The name quantum walk derives from the fact that the evolution can be viewed as a walker scattered randomly on a lattice (here across m numbers). The additional degree of freedom, named as coin corresponding to the polarization in this

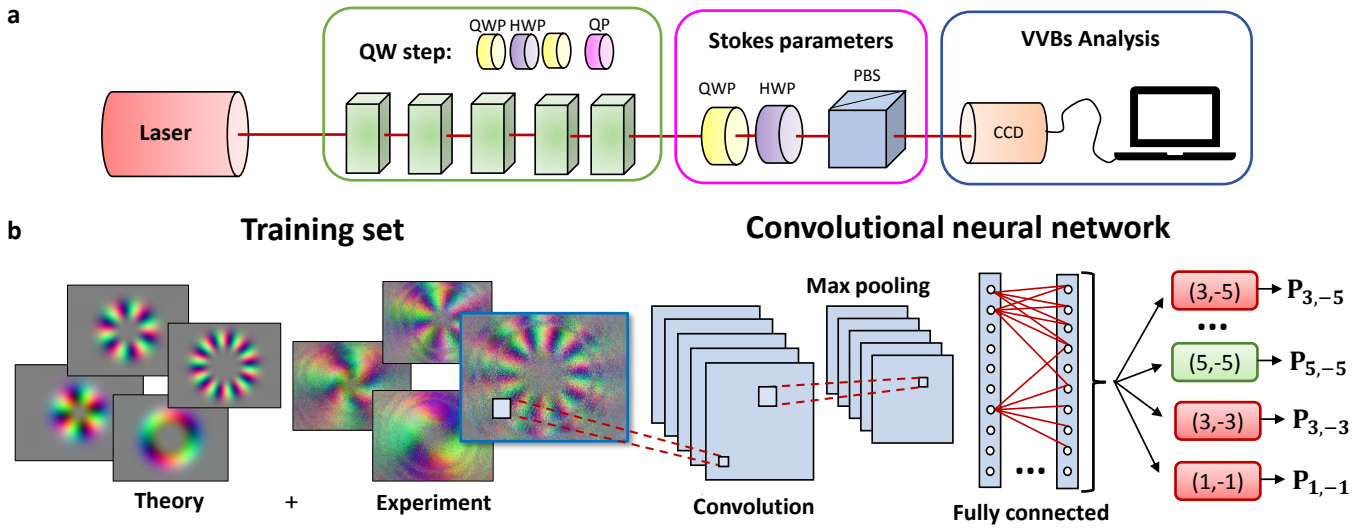

Figure 2. a) Experimental apparatus for the generation of VVBs. A CW laser emits a gaussian beam TEM_{00} at $808nm$. Light passes through series of quantum walks steps made up of waveplates, to manipulate properly the polarization and a q-plate which generates the LG modes. Then we have the detection stage for the measurement of Stokes parameters and the reconstruction of the polarization pattern. This is made possible by the employment of a Charged-Coupled Device (CCD) camera. According to the intensity measured in each pixels of the CCD, Stokes parameters are evaluated and converted in a RGB pictures. b) Conceptual depiction of the working principles of the network. The training set consists of a series of ideal pictures generated with the computer and others collected from the experimental platform. The CNN is made by a series of convolutional and max-pooling layers, ended with a fully connected layer. After the training stage the network is able to classify the pictures recorded in the experiment. Here is reported the recognition of LG modes present in the VVB.

scheme, influences the dynamics making possible the interference among different paths. Then the generation of VVBs as expressed in (1) is performed through a sequence of waveplates, to control polarization, among 5 cascaded q-plates (see Fig.2a). Then a 5-step quantum walk is exploited for generating different classes of VVB states whose order takes the odd values in the interval $[-5, 5]$. The measurement of the polarization pattern is composed by i) a polarization stage realized by cascaded quarter-waveplate, half-waveplate and polarizing beam splitter for obatining the Stokes parameters, and ii) a stage for the measurement of the spatial shape of the beam, realized by a Charged-Coupled Device camera (CCD). In this way it is possible to compute the Stokes parameter for each pixel and to convert the resulting pattern in the RGB color picture. The images are then recognized by the CNN, that will be illustrated in detail in the next section. In Fig.2b is illustrated the training and the classification stages for the problem of demultiplexing m_1 and m_2 orders of the LG modes present in the VVB. It is worth to note that such technique is feasible also in the single-photon regime for quantum optics and information purposes. This is can be made substituting the laser with a single-photon source and using a CCD sensitive to single-photon signal.

Convolutional Neural Network— The CNN is suitable to image classification since it is a translation-invariant network [28]. This feature allow recognition of off-center image and, for example, a flexible use to segmented handwritten digits recognition [29, 30] or to subject independent facial expression recognition [31]. CNN is a form of Feedforward Neural Network and is composed of features extractors and a classifier. The features extractor consists of convolutional and max-pooling layer. The classifier consists of the fully connected layer which performs non-linear transformations of the extracted features. To calculate the convolution at a particular location (x, y), a $k \times k$ region of the input image is multiplied element-by-element with a same size filter and these multiplications are all summed up. Repeating this process for every location on the input image, the output is an activation map of specific features. Typically, more than 1 filter is used in one convolution layer and the outputs are N activation maps. Max-pooling layer is mostly used immediately after the convolutional layer to reduce the spatial size. The output of previous layer are divided into part of $p \times p$ size and maximum operation is applied over every part of the image. Finally, a fully connected layer looks at the output of the previous layer and determines which features most correlate to a particular class. Before the CNN starts, the filter values are randomized. To adjust this values is used backpropagation training process.

In our work, the input images are of size $128 \times 128 \times 3$, where 3 refers to RGB values and we use a CNN with three feature extractors and one classifier. In each convolution layer are used 32 filters of size $3 \times 3 \times 3$ and Rectified Linear Unit (ReLU) activation function. Filters of $2 \times 2 \times 3$ are applied to the outputs of these layers, in max-pooling layers. Finally, the output classification is made up through a fully connected layer which use sigmoid activation function. The network training is made up a finite number of epochs each of which is made up 200 training steps and 100 validation steps.

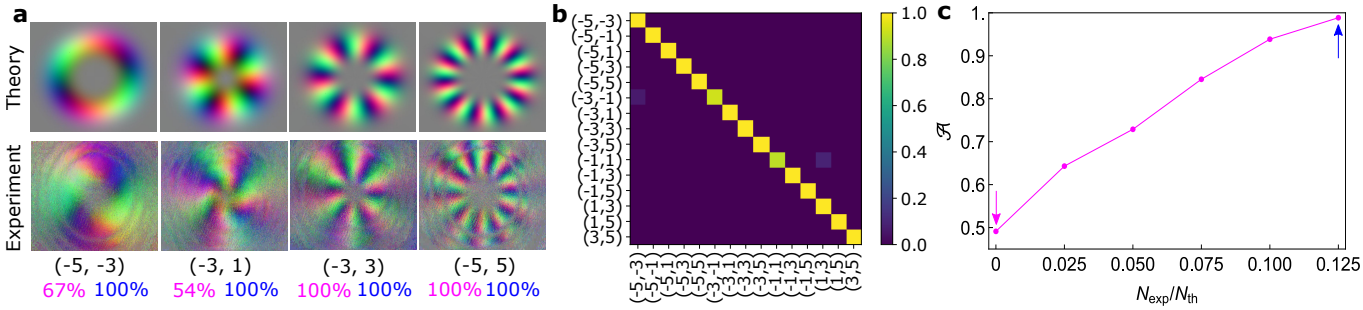

Figure 3. **OAM demultiplexing in VVBs.** a) Comparison between expected and recorded polarization patterns for some VVBs of the ensemble. Below picture the corresponding values (m_1, m_2) and the recognition accuracy by the network, averaged on 100 experimental picture, not included in the training and validation sets, per each class, for two cases. In magenta the accuracy in which the network was trained with theoretical images and with a validation set composed only by experimental pictures. In blue the results with the same validation test and a fraction $N_{exp}/N_{th} = 0.125$ of experimental VVBs in the training set. b) The best true-table $\mathcal{M}$, corresponding to the blue results in a), obtained for the demultiplexing of OAM components for the 15 VVBs that can be generated with a 5-step quantum walk. On raws the possible pairs of the device, on columns the labels assigned by the network. The elements of the matrix have been averaged on 100 experimental images for each class. The mean accuracy per class $\mathcal{A}$, defined as the trace of $\mathcal{M}$ divided per the number of classes, amounts to 0.989. c) Scaling of the mean accuracy per class respect with the fraction of experimental picture in the training set. The points marked with an arrow correspond to the accuracy reported in a).

OAM demultiplexing according to polarization patterns— The platform is feasible to generate all the possible pairs combination between the LG modes of odd orders $m \in [-5, 5]$. We test our network for retrieving the values of m_1 and m_2 after the measurement of polarization, more precisely of the Stokes parameter associated to each pixel. The network is trained firstly with training and test sets consisting of simulated images of the possible VVBs achievable by a 5-step quantum walk. Then the task for the network is to discern between 15 classes. For each class in which $m_1 < m_2$, we have generated states according to (1) with $\theta = \pi/2$ and ϕ varying from 0 to 2π. In this way the size of training set is 400 images per class and 100 for the test set. In this regime the network achieves an accuracy of 100% when tested with theoretical images. However the final goal of this work is to find a reliable technique to classify states generated by the experimental apparatus. To this aim we have collected 100 images for each class from the quantum walk apparatus and used this sample as a validation test for the network. In Fig.3c we have started with a training set made by simulated images. Then, we progressively increase the number of experimental pictures.

Position on the Poincarré sphere— Due to the expression (1) it is possible to retrieve not only the orders (m_1, m_2) but also the values (θ, ϕ) by suitable measurements of polarization and OAM degree of freedom. The problem is analogous of state tomography, that is a crucial topic in quantum information. In our setup we perform a complete set of polarization measurements (projecting on a set of mutually unbiased basis), followed by the recording of the intensity distribution of the beam in the transverse plane. Such measurement stage does not allows for a full reconstruction of the states but can give to the observers, in some special case as VVBs in (1), enough information about the coordinates on the Poincarré sphere.

In this section we test the network to classify each recorded VVB according to the values (θ, ϕ) for the case $|m_1| = |m_2| = 1$. Indeed these VVBs can be unambiguously determined with our measurement stage and by the CNN. High order VVBs display a polarization pattern whose periodicity increases as $\frac{2\pi}{|m_1 - m_2|}$ (see Fig.3a for instance) [6, 7]. Such behaviours makes harder the recognition of ϕ in the images, since a changing in the phase results in a very small rotation of the pattern.

As in the in previous section, the network is trained with ideal patterns for different positions on the sphere. The latter is divided in sectors that covers intervals in which both θ and ϕ varies of $\pi/4$ (see Fig.4a). The sesulting number of classes is 32. [commenti ai risultati ancora mancanti]

Discussion—

Acknowledgements—

[1] L. Jinsong, L. Tongtong, and G. Ling, Optics and Lasers in Engineering **50**, 996 (2012).
[2] W. Tingting, K. Cuifang, H. Xiang, and L. Xu, Optik **124**, 4762 (2013).
[3] Z. Xiaoqiang, C. Ruishan, and W. Anting, Optics Communications **414**, 10 (2018).
[4] S. C. Tidwell, D. H. Ford, , and W. D. Kimura, Applied Optics **29** (1990).
[5] A. V. Nesterov and V. G. Niziev, Journal of Physics D: Applied Physics **33**, 1817 (2000).
[6] R. Fickler, R. Lapkiewicz, W. N. Plick, M. Krenn, C. Schaeff, S. Ramelow, and A. Zeilinger, Science **338** (2012).
[7] V. D'Ambrosio, N. Spagnolo, L. Del Re, S. Slussarenko, Y. Li, L. C. Kwek, L. Marrucci, S. P. Walborn, L. Aolita, and F. Sciarrino, Nature Comm. **4** (2013).
[8] V. D'Ambrosio, E. Nagali, S. P. Walborn, L. Aolita, S. Slussarenko, L. Marrucci, and F. Sciarrino, Nature Comm. **3** (2012).

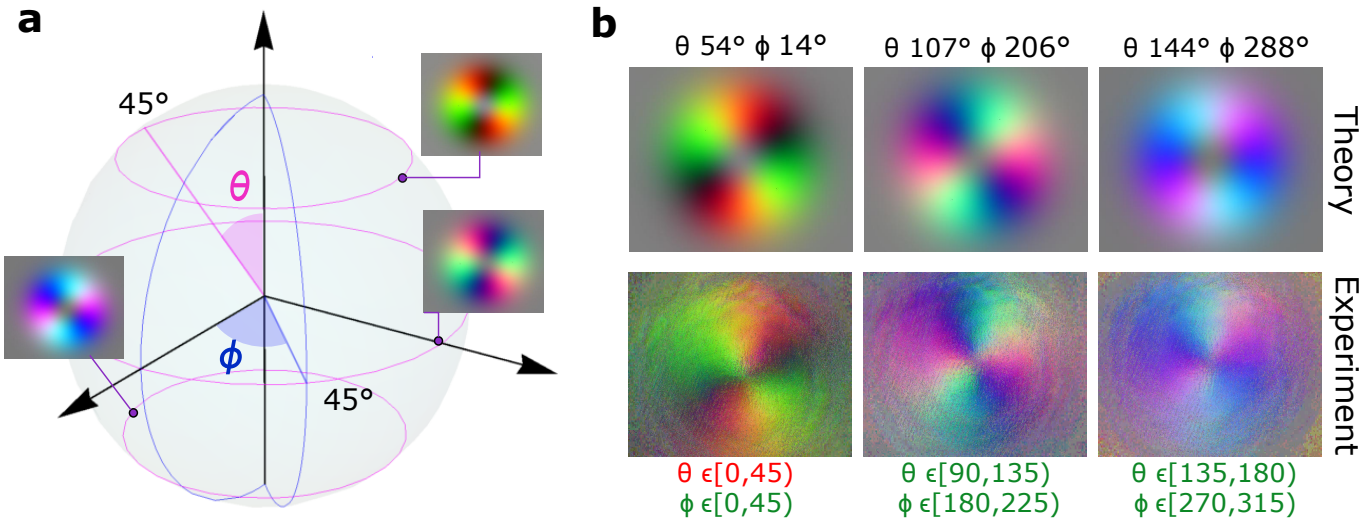

Figure 4. a) Partition of Poincarré sphere in sectors: magenta parallels are the θ intervals; blue meridians the ϕ ones (only the first is shown in the figure). On the surface are reported some VVBs. Along a meridian the colors of the pattern vary from the hottest to the coldest ones. Along a parallel the pattern rotates with a period of π. b) Comparison between experimental VVBs with the expected picture for (θ, ϕ) reported on the top. Below pictures there are the label assigned by the network to the experimental images. We have marked with green the right answers and with red the wrong ones. The network here was trained with the theoretical pictures and a fraction of 0.01 of VVBs taken from the platform.

[9] G. Vallone, V. DAmbrosio, A. Sponselli, S. Slussarenko, L. Marrucci, F. Sciarrino, and P. Villoresi, Phys. Rev. Lett. **113** (2014).

[10] M. Krenn, R. Fickler, M. Fink, J. Handsteiner, M. Malik, T. Scheidl, R. Ursin, and A. Zeilinger, New J. Phys. **9** (2014).

[11] M. Krenn, J. Handsteiner, M. Fink, R. Fickler, R. Ursin, M. Malik, and A. Zeilinger, Proceedings of the National Academy of Sciences , 0027 (2016).

[12] P. Zhang, B. H. Liu, R. F. Liu, H. R. Li, F. L. Li, and G. C. Guo, Physical Review Letters **81** (2010).

[13] F. Cardano, F. Massa, H. Qassim, E. Karimi, S. Slussarenko, D. Paparo, C. de Lisio, F. Sciarrino, E. Santamato, R. W. Boyd, and L. Marrucci, Science Advances **1**, e1500087 (2015).

[14] F. Cardano, M. Maffei, F. Massa, B. Piccirillo, C. de Lisio, G. D. Filippis, V. Cataudella, E. Santamato, and L. Marrucci, Nature Communications **7**, 11439 (2016).

[15] F. Cardano, A. DErrico, A. Dauphin, M. Maffei, B. Piccirillo, C. de Lisio, G. D. Filippis, V. Cataudella, E. Santamato, L. Marrucci, M. Lewenstein, and P. Massignan, Nature Comm. **8** (2017).

[16] T. Giordani, E. Polino, S. Emiliani, A. Suprano, L. Innocenti, H. Majury, L. Marrucci, M. Paternostro, A. Ferraro, N. Spagnolo, and F. Sciarrino, Phys. Rev. Lett. **122**, 020503 (2019).

[17] T. Doster and A. T. Watnik, Appl. Opt. **56**, 3386 (2017).

[18] J. Li, M. Zhang, and D. Wang, IEEE Photonics Technology Letters **29**, 1455 (2017).

[19] S. R. Park, L. Cattell, J. M. Nichols, A. Watnik, T. Doster, and G. K. Rohde, Opt. Express **26**, 4004 (2018).

[20] S. Lohani, E. M. Knutson, M. O'Donnell, S. D. Huver, and R. T. Glasser, Appl. Opt. **57**, 4180 (2018).

[21] S. Lohani and R. T. Glasser, Opt. Lett. **43**, 2611 (2018).

[22] J. Li, M. Zhang, D. Wang, S. Wu, and Y. Zhan, Opt. Express **26**, 10494 (2018).

[23] F. Cardano, E. Karimi, S. Slussarenko, L. Marrucci, C. de Lisio, and E. Santamato, Applied Optics **51** (2012).

[24] L. Allen, M. W. Beijersbergen, R. J. C. Spreeuw, and J. P. Woerdman, Phys. Rev. A **45**, 8185 (1992).

[25] G. Milione, H. I. Sztul, D. A. Nolan, and R. R. Alfano, Phys. Rev. Lett. **107**, 053601 (2011).

[26] L. Marrucci, C. Manzo, and D. Paparo, Physical Review Letters **96**, 163905 (2006).

[27] S. K. Goyal, F. S. Roux, A. Forbes, and T. Konrad, Physical Review Letters **110**, 263602 (2013).

[28] W. Zhang, K. Itoh, J. Tanida, and Y. Ichioka, Appl. Opt. **29**, 4790 (1990).

[29] P. Y. Simard, D. Steinkraus, and J. C. Platt, in *ICDAR* (2003).

[30] D. C. Cireşan, U. Meier, J. Masci, L. M. Gambardella, and J. Schmidhuber, in *Proceedings of the Twenty-Second International Joint Conference on Artificial Intelligence - Volume Volume Two*, IJCAI'11 (AAAI Press, 2011) pp. 1237–1242.

[31] M. Matsugu, K. Mori, Y. Mitari, and Y. Kaneda, Neural Networks **16**, 555 (2003), advances in Neural Networks Research: IJCNN '03.